International Journal of Thermophysics, Vol. 9, No. 5, 1988

Image-Plane Measurements of Coexistence Curve Diameters[1]

D. Balzarini,[2] J. deBruyn,[2] U. Narger,[2] and K. Pang[2]

The diameter of the coexistence curve has been measured for several fluids to determine differences from linear form. The experimental method consists of optical interference measurements in a Mach–Zehnder interferometer supplemented by measurements of deviation in a hollow prism. The fluid sample is contained in a temperature-stabilized cell in one branch of the interferometer. A variation in cell temperature causes the density profile within the cell to change, resulting in a change of the interference pattern, which is monitored photographically. From the relation of this pattern at any temperature to the pattern at the critical temperature, information on the refractive indices of the liquid and vapor phases is obtained. This information is combined with measurements of the Lorentz–Lorenz coefficient to obtain liquid and vapor densities along the coexistence curve. The average of liquid and vapor densities is analyzed in terms of RG theory. The results of the experiment yield information on three body interactions. Studies have been completed on ethane, ethylene, hydrogen, and fluoroform.

KEY WORDS: coexistence curve; critical phenomena; interferometry; ethane; ethylene; hydrogen; fluoroform.

1. INTRODUCTION

The study of phase transitions requires precise measurements to determine the validity of modern theories. Experimental methods using optical techniques are described in this paper for studying the diameter of the coexistence curve of fluids. Modern theories have indicated that the century-old rectilinear law of Cailletet and Matthias is not valid near the critical points [1–7]. Experimental studies have confirmed that a linear law is not

[1] Paper presented at the Tenth Symposium on Thermophysical Properties, June 20–23, 1988, Gaithersburg, Maryland, U.S.A.

[2] Department of Physics, University of British Columbia, Vancouver, B.C. V6T 2A6, Canada.

0195-928X/88/0900-0739$06.00/0

840/9/5-8

adequate to describe the diameter [8–11]. Recent theoretical work has shown that the departures can be accounted for by many-body interactions [12–14].

The densities of coexisting liquid and vapor phases of a pure substance can be related to temperature in the vicinity of the critical point by a power law

$$\Delta\rho^* = \frac{\rho_l - \rho_v}{\rho_c} = B_0 t^\beta \tag{1}$$

where $t = |(T - T_c)/T_c|$ is the reduced temperature, ρ_c is the critical density, and B_0 is a system-dependent constant. The range of validity of this power law was thought to be universal and to extend far from the critical point until two decades ago. Experimental data indicated that the exponent β changed as the temperature varied. Optical experiments reported by Balzarini in 1968 showed that the critical exponent β from xenon changed from a value of 0.355 to 0.339 as the critical temperature was approached [15]. Nuclear magnetic resonance experiments were reported by Stacey et al. in 1969 confirming this variation in β for xenon [16]. Optical measurements on SF_6 also showed this variation in β. These experiments showed different values of β for xenon and SF_6 away from the critical point but the same value close to the critical point [17].

Renormalization group theory predicts that Eq. (1) is insufficient to describe coexisting liquid and vapor densities. It must be modified to include correction-to-scaling terms [18, 19]. Inclusion of these terms yields, for the order parameter,

$$\Delta\rho^* = B_0 t^\beta (1 + B_1 t^\Delta + B_2 t^{2\Delta} + \cdots) \tag{2}$$

where Δ is a universal correction-to-scaling exponent and the amplitudes B_i are system dependent. The value of Δ has been calculated to be close to 0.5 [20–22]. Experimental measurements of this exponent Δ are not trivial because of the interplay of several parameters being fitted but experiments have been consistent with theory [8, 10, 23, 24].

The diameter of the coexistence curve $\rho_d^* = (\rho_l + \rho_v)/2\rho_c$ should behave as

$$\rho_d^* = 1 + A_1 t + A_{1-\alpha} t^{1-\alpha} + \cdots \tag{3}$$

where α is the critical exponent associated with the constant-volume specific heat. The linear term is just the classical term of Cailletet and Matthias. The $t^{1-\alpha}$ term is due to the absence of particle-hole symmetry in real fluids compared with models used in calculating critical behavior. Recently this nonlinear behavior has been explained in terms of many-body interactions [12–14].

2. EXPERIMENTAL

The liquid–vapor coexistence curve diameter experiments performed in this laboratory are done by optical methods. One technique uses a hollow prism for determining the refractive index and changes in the refractive index. The other techniques use focal-plane and image-plane interference for determining changes in the refractive index. Density information is obtained from refractive index measurements by employing the Lorentz–Lorenz relation

$$\frac{n^2-1}{n^2+2}=L\rho \tag{4}$$

where n is the refractive index, ρ is the density, and L is the Lorentz–Lorenz coefficient. L is related to the polarizability and is nearly constant. The slight dependence of L on density is considered in these experiments for any effect it may have on the resulting conclusions.

2.1. Prism Experiment

The prism experiment is similar to earlier experiments [25, 26]. A brief description is given here. A diagram of the optical bench is shown in Fig. 1. The laser is spatially filtered and collimated by a beam-expanding telescope and pinhole filter. The beam is directed through a hollow, prism-shaped sample vessel and into a telescope. The mirror which directs the beam emerging from the prism is driven with a micrometer screw, allowing measurements of small changes of angles of deviation through the prism. Another beam is directed around the sample to permit checks on the optical bench alignment.

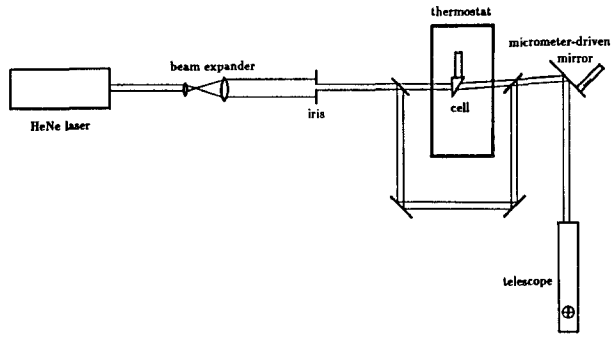

Fig. 1. Schematic diagram of optical equipment used in prism experiments.

The hollow-prism sample vessel is made of aluminum, sapphire windows, brass, a stainless-steel needle valve, and indium seals. The axis of the prism is vertical, giving a horizontal deviation of the laser beam. The micrometer-driven mirror is calibrated with a Ronchi grating and all angles are measured with reference to the angle measured with air in the cell. The angles of deviation of beams traversing the liquid and vapor portions of the sample are measured as a function of temperature. The index of refraction of the liquid and vapor and the coexisting densities are then calculated. Experimental difficulties are encounted near the critical temperature because gravitational rounding of the meniscus smears the image in the telescope. It should be pointed out that this same experimental apparatus is used for studying the variation in the Lorentz–Lorenz coefficient [27].

2.2. Image-Plane Interference

A schematic diagram of the optical bench apparatus is shown in Fig. 2. A laser is filtered, expanded, and collimated by a pinhole and lenses. The beam is split in a Mach–Zehnder interferometer. One beam traverses the sample cell and the other serves as a reference beam. A lens follows the beam combiner. Marked on the diagram are the focal plane and the image plane.

The sample fluid is contained in a vessel with parallel sapphire windows. The sample vessel is mounted in a copper block which is wrapped with heating wire. Thermistors and a quartz thermometer probe are embedded in the block and are used to control and monitor the temperature. The error signal from a DC bridge is processed and used to

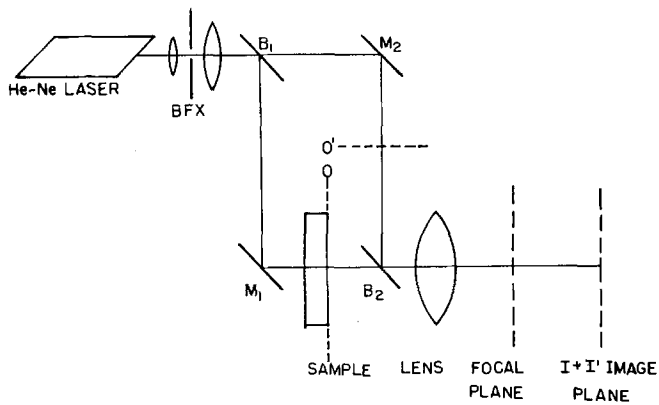

Fig. 2. Schematic diagram of optical equipment used in interference experiments.

control the amount of heat input to the resistance wire wrapping on the block. The block is insulated with styrofoam from an outer jacket which is temperature controlled using water circulated from a regulated bath. The resulting temperature control on the copper block holding the sample vessel is 0.0001 K.

The large compressibility of the fluid near the critical temperature results in a large gravitational density gradient in the sample. This density distribution is sigmoid in shape when the temperature is above the critical temperature. This shape is illustrated in Fig. 3 by the curve marked $T \lesssim T_c$. Interference between the sample beam and the reference beam is photographed in the image plane. The interference pattern consists of horizontal fringes which are closely spaced where the density gradient is largest and more widely spaced where the gradient is smaller. Measurements of near-critical isotherms using image-plane interference were reported previously [28].

The density distribution in the sample for temperatures well above critical is uniform as shown in Fig. 3, labeled $T \gg T_c$. The image-plane

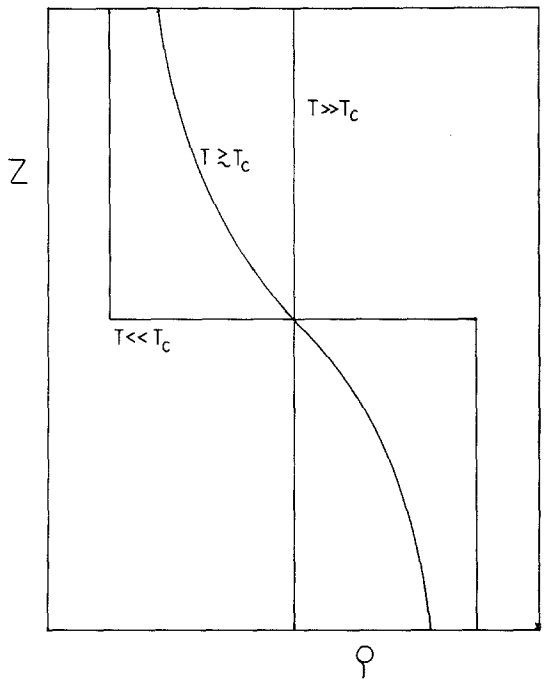

Fig. 3. Density versus height distribution in the sample cell for temperatures near critical, far above critical, and far below critical.

pattern in this case is a uniform field if the interferometer is perfectly aligned. The intensity of the field depends on the phase difference between the sample beam and the reference beam. The density distribution in the sample for temperatures well below critical consists of two uniform regions separated by a relatively sharp meniscus. The image-plane pattern for this case consists of two uniform regions, the intensity of each depending on the phase difference between that part of the sample beam and the reference beam. In between these two regions are many closely packed fringes corresponding to the meniscus.

It should be pointed out that the foregoing description of image-plane interference patterns assumed perfect alignment of the interferometer. In practice, it is often desirable to misalign it slightly to produce a few horizontal fringes. The effects of the misalignment must be subtracted from the image-plane patterns in data analysis. One reason for misaligning is to prevent the possibility of overcounting a fringe. Consider, for example, a uniform field and an increasing phase difference. If the phase difference were always increasing, the resulting image-plane intensity alternates between dark and light. This cannot be distinguished from what would be observed if the changing phase difference reversed when it reached a maximum or a minimum. The introduction of a few fringes by misalignment alleviates this problem. Phase difference reversals are then noticeable on the photographic strip recording the data.

Illustrations of the image-plane interference pattern for various temperatures are shown in Fig. 4. Data are taken by scanning the temperature as a photographic record is made in a narrow vertical slice of the image plane. The temperature is scanned in steps by controlled sweep-and-stop periods. As the temperature increases from far below critical, fringes emerge from the "meniscus" into the liquid and vapor regions. This continues until the sample is above the critical temperature. Measurements on the film record are made of optical phases corresponding to the liquid and vapor edges of the meniscus and then compared with the optical phase corresponding to the critical density. Let these phases be labeled N_l, N_v, and N_c. Data analysis relates these to the corresponding densities ρ_l, ρ_v, and ρ_c using the cell thickness, laser wavelength, and Lorentz–Lorenz relation.

The difference between ρ_l and ρ_v as a function of temperature yields coexistence curve information. Analysis of this difference yields the critical temperature, critical exponents, and amplitudes. The average of ρ_l and ρ_v yields the coexistence curve diameter.

Care must be taken in these experiments to prevent the optical path lengths of the interferometer arms from changing due to other causes. For example, room-temperature changes could introduce overall fringe changes

in the image-plane patterns which could be interpreted as changes in the diameter. In addition to trying to minimize any extraneous effects, it is useful to run through complete temperature scans with an empty cell to check for possible sources of error.

2.3. Focal-Plane Interference

The interference produced in the focal plane of the lens is used to study the coexisting density differences, compressibilities, and isotherms [15, 29]. (An assumption about antisymmetry of the isotherms must be made, however.) The interference fringes in the focal plane are produced by rays which traverse equal-gradient regions in the sample above and below

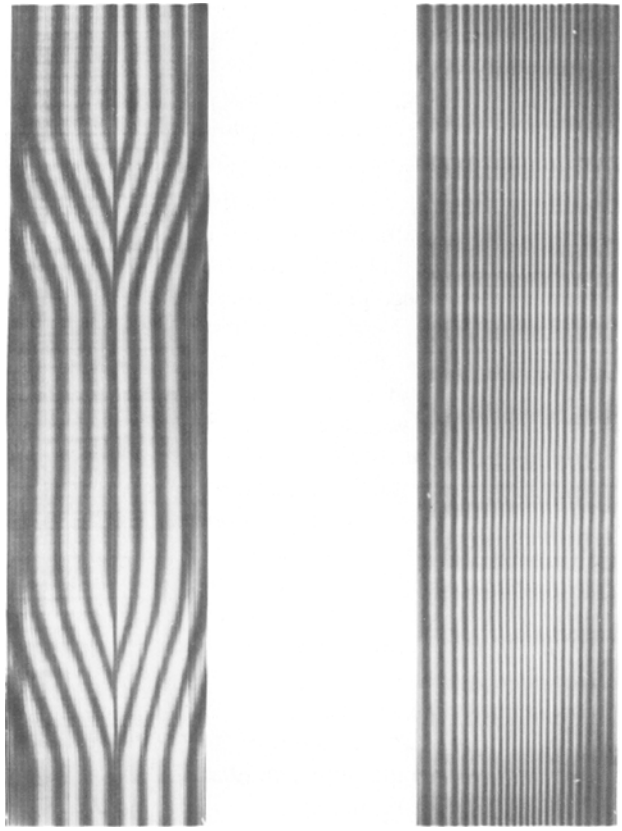

Fig. 4. The interference pattern obtained by photographing the image plane as the temperature is changed.

the highest gradient region. Although refracted to the same position in the focal plane, they differ in phase in general. Missing fringes in the focal-plane pattern yield information on the density difference between liquid and vapor as a function of temperature. Focal-plane interference is used in the work reported in this paper to confirm results obtained with the prism technique and the image-plane interference technique when the focal-plane technique yields the same information. The density difference along the coexistence curve and the critical temperature are examples. No information about the diameter is obtainable from focal-plane interference.

3. RESULTS

The coexistence curve diameters of ethane, ethylene, hydrogen, and fluoroform have been examined in these experiments. The prism technique was used for ethane and ethylene. Image-plane interference was used for hydrogen and was the main technique used for fluoroform. Results for these fluids are shown in Fig. 5, where coexistence curve diameters versus reduced temperatures are plotted. The dashed lines correspond to linear fits to the diameter data away from the critical point. The data clearly show a

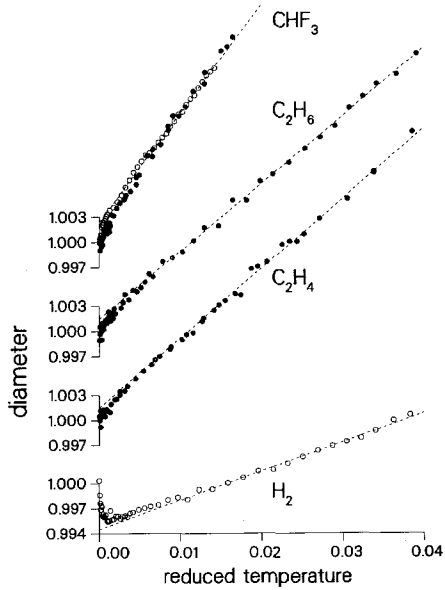

Fig. 5. Coexistence curve diameters as functions of reduced temperatures for CHF_3, C_2H_6, C_2H_4, and H_2. Dashed lines indicate linear fits to the data for $t > 0.008$.

departure from linear behavior. The departure from linear behavior of the H_2 data is in the opposite direction to that of the other fluids.

Some of these data were analyzed along with data for Ne and N_2 of Pestak and Chan [8] and data for SF_6 of Weiner et al. [11] in recent papers [12, 13]. The departures from linear behavior are ascribed to the effect of repulsive, many-body forces. The deviation of the data for hydrogen in the opposite direction from the data for other fluids suggests that the forces in that case are attractive rather than repulsive [23, 30].

This image-plane interference technique allows data to be obtained fairly close to the critical point. The experiment does not depend on determinations of ρ_c from other experiments. Other experimental techniques such as capacitance measurements allow more precision in making measurements but this optical technique allows measurements closer to the critical point. It would be interesting to do a combined capacitance and optical experiment on the same samples.

REFERENCES

1. L. Cailletet and E. Matthias, *C.R. Acad. Sci.* **102**:1202 (1886); *C.R. Acad. Sci.* **104**:1563 (1887).
2. N. D. Mermin, *Phys. Rev. Lett.* **26**:169 (1971); *Phys. Rev. Lett.* **26**:957 (1971).
3. G. W. Mulholland, J. A. Zollweg, and J. M. H. Levelt-Sengers, *J. Chem. Phys.* **62**:2535 (1975).
4. B. Widom and J. S. Rowlinson, *J. Chem. Phys.* **52**:1670 (1970); J. S. Rowlinson, *Adv. Chem. Phys.* **41**:1 (1980); P. C. Hemmer and G. Stell, *Phys. Rev. Lett.* **24**:1284 (1970).
5. J. J. Rehr and N. D. Mermin, *Phys. Rev.* **A8**:472 (1973).
6. N. D. Mermin and J. J. Rehr, *Phys. Rev.* **A4**:2408 (1971).
7. J. F. Nicoll, *Phys. Rev.* **A24**:2203 (1981); J. F. Nicoll and R. K. P. Zia, *Phys. Rev.* **B23**:6157 (1981); J. F. Nicoll and P. C. Albright, in *Proceedings of the Eight Symposium on Thermophysical Properties*, J. V. Sengers, ed. (American Society of Mechanical Engineers, New York, 1982), Vol. I, p. 377.
8. M. W. Pestak, Ph.D. thesis (The Pennsylvania State University, University Park, 1983) (unpublished); M. W. Pestak and M. H. W. Chan, *Phys. Rev.* **B30**:274 (1984); *Bull. Am. Phys. Soc.* **29**:227 (1984).
9. M. Burton and D. Balzarini, *Can. J. Phys.* **52**:2011 (1974); D. Balzarini and M. Burton, *Can. J. Phys.* **57**:1516 (1979).
10. J. R. deBruyn and D. A. Balzarini, *Phys. Rev.* **A36**:5677 (1987).
11. J. Weiner, K. H. Langley, and N. C. Ford, Jr., *Phys. Rev. Lett.* **32**:879 (1974); J. Weiner, Ph.D. thesis (University of Massachusetts, Amherst, 1974) (unpublished).
12. R. E. Goldstein, A. Parola, N. W. Ashcroft, M. W. Pestak, M. H. W. Chan, J. R. deBruyn, and D. A. Balzarini, *Phys. Rev. Lett.* **58**:41 (1987).
13. M. W. Pestak, R. E. Goldstein, M. H. W. Chan, J. R. deBruyn, D. A. Balzarini, and N. W. Ashcroft, *Phys. Rev.* **B36**:599 (1987).
14. R. E. Goldstein and A. Parola, In press.
15. D. Balzarini, Ph.D. thesis (Columbia University, New York, 1968).
16. L. M. Stacey, B. Pass, and H. Y. Carr, *Phys. Rev. Lett.* **23**:1424 (1969).
17. D. Balzarini and K. Ohrn, *Phys. Rev. Lett.* **29**:840 (1972).

18. F. J. Wegner, *Phys. Rev.* **B5**:4529 (1972).
19. M. Ley-Koo and M. S. Green, *Phys. Rev.* **A23**:2650 (1981).
20. J. C. LeGuillou and J. Zinn-Justin, *Phys. Rev. Lett.* **39**:95 (1977); *Phys. Rev.* **B21**:3976 (1980).
21. M. J. George and J. J. Rehr, *Phys. Rev. Lett.* **53**:2063 (1984).
22. J. H. Chen, M. E. Fisher, and B. G. Nickel, *Phys. Rev. Lett.* **48**:630 (1982).
23. J. R. deBruyn, Ph.D. thesis (University of British Columbia, Vancouver, 1987).
24. D. Balzarini and O. G. Mouritsen, *Phys. Rev.* **A28**:3515 (1983).
25. H. L. Lorentzen, *Acta Chem. Scand.* **7**:1335 (1953).
26. E. H. W. Schmidt and K. Traube, *Progress in International Research on Thermodynamics, ASME* (Academic Press, New York, 1962).
27. D. Balzarini and P. Palffy, *Can. J. Phys.* **52**:2007 (1974); M. Burton and D. Balzarini, *Can. J. Phys.* **52**:2010 (1974).
28. D. Balzarini, *Can. J. Phys.* **50**:2194 (1972).
29. L. R. Wilcox and D. Balzarini, *J. Chem. Phys.* **48**:753 (1968).
30. J. R. deBruyn and D. Balzarini, In press.